
Article:
Hua, L., Deng, J., Qian, D. et al. (2 more authors) (2016) Modeling and application of ring stiffness condition for radial-axial ring rolling. International Journal of Machine Tools and Manufacture, 110. pp. 66-79. ISSN 0890-6955

https://doi.org/10.1016/j.ijmachtools.2016.09.003

International Journal of Machine Tools & Manufacture, Vol. 110 (2016), pp. 66-79

http://dx.doi.org/10.1016/j.ijmachtools.2016.09.003

Modeling and application of ring stiffness condition for radial-axial ring rolling

Lin Hua[a, c], Jiadong Deng[a, c], Dongsheng Qian[b, c*], Jian Lan[a, c], Hui Long[d]

[a] School of Automotive Engineering, Wuhan University of Technology, Wuhan 430070, China
[b] School of Materials Science and Engineering, Wuhan University of Technology, Wuhan 430070, China
[c] Hubei Key Laboratory of Advanced Technology for Automotive Components, Wuhan 430070, China
[d] Department of Mechanical Engineering, The University of Sheffield, Sheffield S1 3JD, UK

* Corresponding author at: Wuhan University of Technology, Wuhan 430070, China.
E-mail address: qiands@whut.edu.cn (D. Qian).

Abstract

Radial-axial ring rolling (RARR) is an advanced rotary forming technology for manufacturing various seamless rings, especially for large scale rings. A primary problem for RARR is to facilitate rolling process stability and form a ring with good dimension and performance. However, RARR is an extremely complex dynamic rolling process with high flexibility. To reasonably control guide roll is an important approach to keep rolling process stable during RARR. In this paper, a mathematical model of ring stiffness condition for RARR was established based on the force method. Then the influence factors to ring stiffness were discussed, especially the section bending moment factor. To verify the ring stiffness model, finite element (FE) simulation was adopted. In addition, a comparison of different ring stiffness models was made. It can be found the proposed stiffness model has a high accuracy. Furthermore, a control method of the pressure in the hydraulic cylinder to adjust the guiding force based on the stiffness model was proposed. By FE simulation of RARR, an appropriate adjustment coefficient to determine the guiding force was obtained. Finally, an experiment of RARR for a large ring was carried out. The rolling process was very smooth and steady, and a super-large ring with diameter more than 9 meters was manufactured successfully.

Keywords: Radial-axial ring rolling; Guide roll; Ring stiffness condition; Mathematical modeling; Guiding force.

International Journal of Machine Tools & Manufacture, 110 (2016) 66-79
http://dx.doi.org/10.1016/j.ijmachtools.2016.09.003

1 Introduction

Ring rolling is an advanced rotary forming technology to manufacture seamless rings, such as bearing races, ring gears, flanges, aero-engine casings, etc. Compared with traditional manufacturing technologies, it has advantages of high producing efficiency and processing precision, low energy consumption and material cost, good microstructure and performance. Over 160 years, ring rolling has evolved into a relatively mature technology [1, 2], with amount of research work in theory [3-6], technique [7-10] and equipment [11, 12].

As a typical ring rolling method, RARR is suited to manufacture large scale rings at high temperature. During RARR, as shown in Fig. 1, the thickness of a ring is reduced by the radial extrusion of the main roll and mandrel, and the height is reduced by the axial extrusion of the upper and lower conical rolls. In radial deformation area, the main roll makes active rotary motion and the mandrel makes radial feed movement. In axial deformation area, the upper conical roll makes downward feed movement and the two conical rolls both make active rotary motion. When the thickness and height of the ring reduce, the diameter of the ring enlarges. The two conical roll also move backwards to keep them contact with the ring surface during rolling process. The two guide rolls are arranged respectively in the two sides of the main roll to steer the ring and keep the rolling process stable.

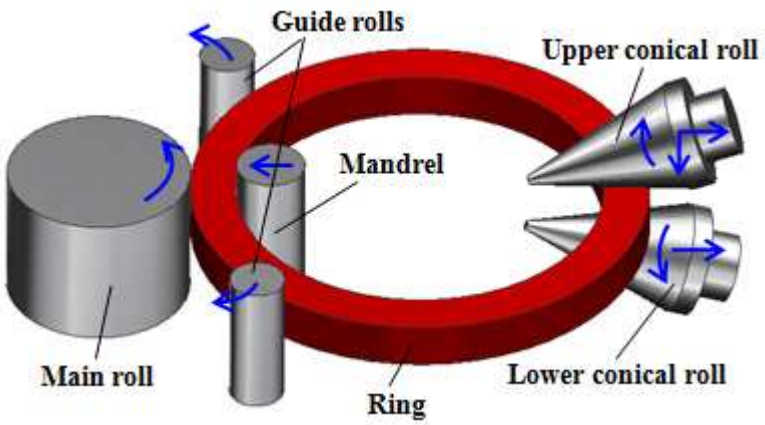

Fig. 1. Forming principle of RARR

From the forming principle of RARR above, it can be seen that RARR is an extremely complex dynamic rolling process with high flexibility. Recently, researches on RARR are mainly focused on FE modeling method and process simulation. For instance, Xie et.al [13] developed a rigid–viscoplastic dynamic explicit finite element code to simulate ring rolling. Davey and Ward [14] proposed a practical method for FE simulation of RARR using ALE flow formulation instead of conventional Lagrangian approach. Kim et al. [15] put forward a dua-mesh approach to RARR simulation with high computational efficiency. Simulations of microstructure evolution during RARR have been also tried [16-18]. By FE simulation, deformation behaviors during RARR and effects of technological parameters on RARR process have been revealed systematically [19-23]. Besides, macro–microscopic deformation laws during blank forging and ring rolling process have been investigated [24].

To facilitate rolling process stable and form a ring with good dimension and performance, some rolling conditions have been proposed. To make the ring rotate smoothly, biting condition in radial and axial rolls should be satisfied [25]. To make the ring produce plastic deformation, the penetrating condition in radial and axial deformation areas should be met [25]. Furthermore, to make rolling process stable, a steady forming condition for RARR should be guaranteed [26]. In the process of real manufacturing, waste ring product with distorted shape is an important problem, as shown in Fig. 2. One key reason is that the force applied on the guide roll is inappropriate.

Fig. 2. Waste ring products with distorted shape

At present, some scholars have made studies on the guide roll of ring rolling. Hua et al. [27] adopted a theoretical method to predict the motion rule of guide roll by calculating the ring size during cold radial ring rolling process of a groove ball ring. Li et al. [28] proposed a method to control the guide rolls by adjusting the pressure of hydraulic mechanism in 3D-FE radial ring rolling simulation. Xu et al. [29] put forward a plastic instability criterion for radial ring rolling and calculated the bending moment of ring under the action of guide rolls by the force method. Forouzan et al. [30] put forward employing thermal spokes method to simulate the guide roll effect in FE analysis of radial ring rolling process. However, compared with radial ring rolling, the rolling system of RARR is more complex. A pair of conical rolls is involved in the deformation and formed rings are in big size. Therefore, it is more important for RARR to control the guide rolls. Xu et al. [31] adopted the limit analysis method to establish the relationship between the allowed maximum force and the angle of the guide roll, and pointed out the most suitable angle of the guide roll. Hua et al. [32] proposed a ring stiffness condition for RARR, but it made a simplification to calculate the bending moment and emphasized on the permitting maximum outer radius of a ring. However, the research emphases above were not on how to control the force of guide roll based on the guide roll system of RARR.

This study aims to provide a scientific theoretical basis and reliable control method of guide roll during RARR. Firstly, a mathematical model of ring stiffness condition for RARR was established based on the force method. Then the influence factors to ring stiffness were discussed and the predicted results were compared with FE simulation and other ring stiffness models. Finally, a control method of the pressure in the hydraulic cylinder to adjust the guiding force based on the stiffness model was proposed and applied in a RARR experiment of a super-large ring successfully.

International Journal of Machine Tools & Manufacture, 110 (2016) 66-79
http://dx.doi.org/10.1016/j.ijmachtools.2016.09.003

2 Mathematical modeling of ring stiffness condition for RARR

2.1 Establishment of the ring stiffness model

During RARR, the ring is deformed under the pressure of the main roll and mandrel in the radial direction and the pressure of the two conical rolls in the axial direction. Assuming the rotational motions are ignored, the mechanical model for RARR can be regarded as a circular beam with rectangular section fixed in the radial deformation area A and axial deformation area B, as shown in Fig. 3(a). The pressure of the guide roll applied on the ring is simplified as a concentrated force F_g pointing to the center of the circle. To simplify the model, the forces of the two guide rolls are supposed to be equal and the cross-sections of the rolled ring are supposed to be unified. Thus, it is a symmetric model, and a half model can be used to analyze the mechanical condition, as shown in Fig. 3(b). It is a three times statically indeterminate structure. Generally, the force method and displacement method are two basic and effective means to calculate statically indeterminate structures. In this paper, the force method is selected to analyze the mechanical condition. Based on the force method, the fixed joint at section B is removed and equivalent support reaction is added, as shown in Fig .4. X_1, X_2 are the support forces in horizontal and vertical directions respectively, and M_3 is the support moment.

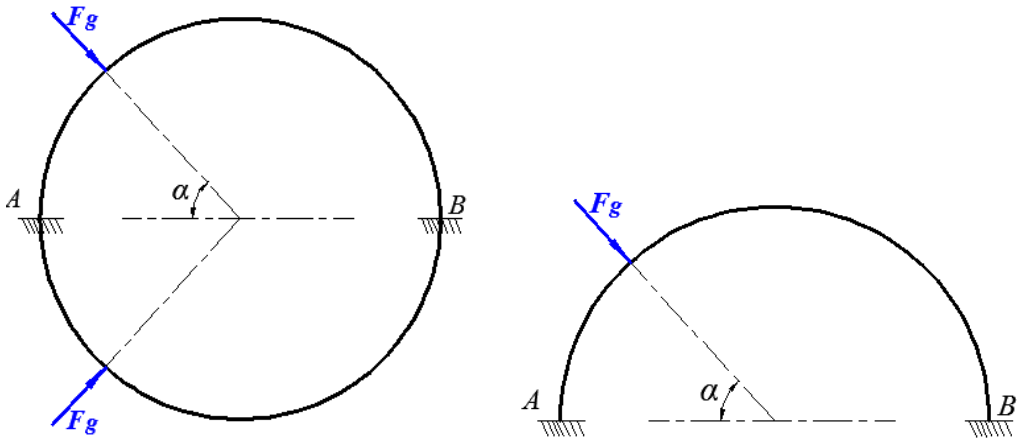

Fig. 3. Simplified sketch of mechanical model for RARR: (a) a complete model; (b) a half model.

International Journal of Machine Tools & Manufacture, 110 (2016) 66-79
http://dx.doi.org/10.1016/j.ijmachtools.2016.09.003

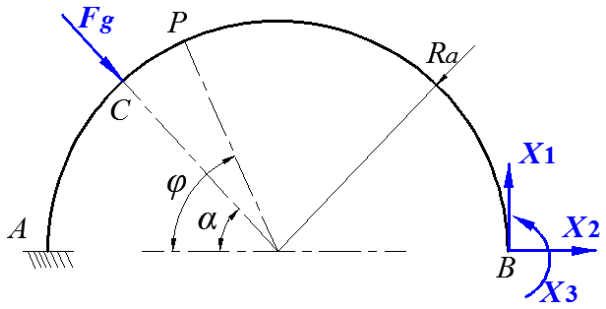

Fig. 4. Equivalent mechanical model based on the force method

Firstly, the section bending moment of the circular beam caused by each force should be obtained. The section bending moment of the circular beam $M_g(\varphi)$ caused by the guiding force F_g can be defined as

$$M_g(\varphi)=\begin{cases}0 & (0\le\varphi<\alpha)\\ F_g R_a \sin(\alpha-\varphi) & (\alpha<\varphi\le\pi)\end{cases} \tag{1}$$

where R_a is the average diameter of the rolled ring, the section P is an any section on the beam and φ is the central angle of the arc $\overset{\frown}{AP}$, α is the position angle of guide roll.

Then the section bending moment of the circular beam $\overline{M_1}(\varphi)$ caused by the unit load $\overline{X_1}$ in the same direction as X_1 can be expressed as

$$\overline{M_1}(\varphi)=-R_a(1+\cos\varphi) \qquad (0\le\alpha\le\pi) \tag{2}$$

The section bending moment of the circular beam $\overline{M_2}(\varphi)$ caused by the unit load $\overline{X_2}$ in the same direction as X_2 can be expressed as

$$\overline{M_2}(\varphi)=-R_a\sin\varphi \qquad (0\le\alpha\le\pi) \tag{3}$$

The section bending moment of the circular beam $\overline{M_3}(\varphi)$ caused by the unit load $\overline{X_3}$ in the same direction as X_3 can be expressed as

$$\overline{M_3}(\varphi)=-1 \qquad (0\le\alpha\le\pi) \tag{4}$$

Then the generalized displacement caused by each force at section B should be calculated. The generalized displacement Δ_{1g} caused by F_g at the section B in the same direction as X_1 can be calculated by

$$\Delta_{1g}=\int_0^{\pi}\frac{M_g(\varphi)\overline{M_1}(\varphi)}{EI}R_a d\varphi=-\frac{F_g R_a^{\ 3}}{EI}[\frac{1}{4}\cos\alpha(\cos 2\alpha-1)+\frac{1}{4}\sin\alpha\sin 2\alpha+\frac{1}{2}\alpha\sin\alpha+1-\cos\alpha] \tag{5}$$

where E is the elastic modulus, I is the inertia moment.

The generalized displacement Δ_{2g} caused by F_g at the section B in the same direction as X_2 can be calculated by

$$\Delta_{2g}=\int_0^{\pi}\frac{M_g(\varphi)\overline{M_2}(\varphi)}{EI}R_a d\varphi=-\frac{F_g R_a^{\ 3}}{EI}[-\frac{1}{4}\sin\alpha(\cos 2\alpha-1)+\frac{1}{4}\cos\alpha\sin 2\alpha-\frac{1}{2}\alpha\cos\alpha] \tag{6}$$

The generalized displacement Δ_{3g} caused by F_g at the section B in the same direction as X_3 can be calculated by

$$\Delta_{3g}=\int_0^{\pi}\frac{M_g(\varphi)\overline{M_3}(\varphi)}{EI}R_a d\varphi=\frac{F_g R_a^{\ 3}}{EI}(\cos\alpha-1) \tag{7}$$

The generalized displacement δ_{11} caused by $\overline{X_1}$ at the section B in the same direction as X_1 can be calculated by

$$\delta_{11}=\int_0^{\pi}\frac{\overline{M_1}(\varphi)\overline{M_1}(\varphi)}{EI}R_a d\varphi=\frac{2\pi R_a^{\ 3}}{3EI} \tag{8}$$

The generalized displacement δ_{22} caused by $\overline{X_2}$ at the section B in the same direction as X_2 can be calculated by

$$\delta_{22}=\int_0^{\pi}\frac{\overline{M_2}(\varphi)\overline{M_2}(\varphi)}{EI}R_a d\varphi=\frac{\pi R_a^{\ 3}}{2EI} \tag{9}$$

The generalized displacement δ_{33} caused by $\overline{X_3}$ at the section B in the same direction as X_3 can be calculated by

$$\delta_{33}=\int_0^{\pi}\frac{\overline{M_3}(\varphi)\overline{M_3}(\varphi)}{EI}R_a d\varphi=\frac{\pi R_a}{EI} \tag{10}$$

The generalized displacement δ_{12} caused by $\overline{X_2}$ at the section B in the same direction as X_1 is equal to the generalized displacement δ_{21} caused by $\overline{X_1}$ at the section B in the same direction as X_2, and can be calculated by

$$\delta_{12}=\delta_{21}=\int_0^{\pi}\frac{\overline{M_1}(\varphi)\overline{M_2}(\varphi)}{EI}R_a d\varphi=\frac{2R_a^{\ 3}}{EI} \tag{11}$$

The generalized displacement δ_{13} caused by $\overline{X_3}$ at the section B in the same direction as X_1 is equal to the generalized displacement δ_{31} caused by $\overline{X_1}$ at the section B in the same direction as X_3, and can be calculated by

$$\delta_{13}=\delta_{31}=\int_0^{\pi}\frac{\overline{M_1}(\varphi)\overline{M_3}(\varphi)}{EI}R_a d\varphi=\frac{\pi R_a^{\ 2}}{EI} \tag{12}$$

The generalized displacement δ_{23} caused by $\overline{X_3}$ at the section B in the same direction as X_2 is equal to the generalized displacement δ_{32} caused by $\overline{X_2}$ at the section B in the same direction as X_3, and can be calculated by

$$\delta_{23}=\delta_{32}=\int_0^{\pi}\frac{\overline{M_2}(\varphi)\overline{M_3}(\varphi)}{EI}R_a d\varphi=\frac{2R_a^{\ 2}}{EI} \tag{13}$$

Based on the force method, the regular equation of this three times statically indeterminate structure can be expressed as

$$\begin{cases}\delta_{11}X_1+\delta_{12}X_2+\delta_{13}X_3+\Delta_{1g}=0\\ \delta_{21}X_1+\delta_{22}X_2+\delta_{23}X_3+\Delta_{2g}=0\\ \delta_{31}X_1+\delta_{32}X_2+\delta_{33}X_3+\Delta_{3g}=0\end{cases} \tag{14}$$

Then the equivalent support reaction at section B can be obtained

$$X_1=\frac{1}{\pi}F_g\alpha\sin\alpha \tag{15}$$

$$\begin{aligned}X_2=-\frac{1}{2R_a}[&F_gR_a\alpha\sin\alpha+\pi F_gR_a(\frac{\pi}{8-\pi^2}\cos\alpha-\frac{\pi}{8-\pi^2}-\frac{2}{8-\pi^2}\alpha\cos\alpha\\ &+\frac{2}{8-\pi^2}\sin\alpha-\frac{1}{\pi}\alpha\sin\alpha)+F_gR_a(\cos\alpha-1)]\end{aligned} \tag{16}$$

$$X_3=F_gR_a(\frac{\pi}{8-\pi^2}\cos\alpha-\frac{\pi}{8-\pi^2}-\frac{2}{8-\pi^2}\alpha\cos\alpha+\frac{2}{8-\pi^2}\sin\alpha-\frac{1}{\pi}\alpha\sin\alpha) \tag{17}$$

Finally, the section bending moment of the circular beam at section P can be calculated by

$$M_{(\varphi)}=F_gR_aQ_{(\varphi,\alpha)} \tag{18}$$

where $Q_{(\varphi,\alpha)}$ is the section bending moment factor and it can be expressed as

$$Q_{(\varphi,\alpha)}=\begin{cases}\sin(\alpha-\varphi)-\dfrac{\alpha\sin\alpha\cos\varphi}{\pi}-\dfrac{(1-\cos\alpha)\sin\varphi}{2} & \\ +\dfrac{\pi(\pi\cos\alpha-\pi-2\alpha\cos\alpha+2\sin\alpha)\sin\varphi}{2(8-\pi^2)}-\dfrac{\pi\cos\alpha-\pi-2\alpha\cos\alpha+2\sin\alpha}{8-\pi^2} & (0\le\varphi<\alpha)\\ -\dfrac{\alpha\sin\alpha\cos\varphi}{\pi}-\dfrac{(1-\cos\alpha)\sin\varphi}{2} & \\ +\dfrac{\pi(\pi\cos\alpha-\pi-2\alpha\cos\alpha+2\sin\alpha)\sin\varphi}{2(8-\pi^2)}-\dfrac{\pi\cos\alpha-\pi-2\alpha\cos\alpha+2\sin\alpha}{8-\pi^2} & (\alpha<\varphi\le\pi)\end{cases} \tag{19}$$

Then the section bending stress σ can be calculated by the following formula

$$\sigma=\frac{M_{(\varphi)}}{W_z}=\frac{6R_aF_gQ_{(\alpha,\varphi)}}{BH^2} \tag{20}$$

To satisfy the stiffness condition, the maximum section bending stress should satisfy the following expression

$$\sigma_{max}=\frac{\left|M_{(\varphi)}\right|_{max}}{W_z}=\frac{6R_aF_g\left|Q_{(\alpha,\varphi)}\right|_{max}}{BH^2}\le[\sigma]=\sigma_s \tag{21}$$

Thus, to avoid distorting the ring shape, the guiding force should satisfy the stiffness condition

$$F_g\le F_{g-max}=\frac{BH^2\sigma_s}{6R_a\left|Q_{(\alpha,\varphi)}\right|_{max}} \tag{22}$$

2.2 Discussion of the ring stiffness model

According to Eq. (22), the ring stiffness condition in RARR is related to its geometric dimension and yield strength, and also has relation with the maximal absolute valve of the section bending moment factor $\left|Q_{(\alpha,\varphi)}\right|_{max}$. Bigger geometric dimension of ring cross section, smaller geometric dimension of ring radius and bigger yield strength of ring material can make the ring to bear bigger force before being distorted, which are good for improving the ring stiffness. As we can see from Eq. (19), the expression of the section bending moment factor $Q_{(\varphi,\alpha)}$ is related to the position angle of guide roll α and the angle of ring section position φ, but the detail is not clear. Therefore, a further study on the section bending moment factor $Q_{(\varphi,\alpha)}$ is made in this section. The Fig .5 shows a simple relation between $Q_{(\varphi,\alpha)}$, α and φ. It can be seen that the distribution of $Q_{(\varphi,\alpha)}$

along the ring section changes from state I to state II when α increases. That is to say, when α is smaller than a certain valve, the distribution state of $Q_{(\varphi,\alpha)}$ likes an inverted letter N. The maximal absolute valve of the section bending moment factor $\left|Q_{(\alpha,\varphi)}\right|_{\max}$ may only occur in section A, section B, section C or section D. Section A is between the main roll and mandrel in the ring. The absolute valve of the section bending moment factor at section A can be expressed as

$$\left|Q_{(\alpha,0)}\right|=\left|\sin\alpha-\frac{\alpha\sin\alpha}{\pi}-\frac{\pi\cos\alpha-\pi-2\alpha\cos\alpha+2\sin\alpha}{8-\pi^2}\right| \tag{23}$$

Section B is between the two conical rolls in the ring. The absolute valve of the section bending moment factor at section B can be calculated by

$$\left|Q_{(\pi,\alpha)}\right|=\left|\frac{\alpha\sin\alpha}{\pi}-\frac{\pi\cos\alpha-\pi-2\alpha\cos\alpha+2\sin\alpha}{8-\pi^2}\right| \tag{24}$$

Section C is contacted with the guide roll in the ring. The absolute valve of the section bending moment factor at section C can be determined by

$$\left|Q_{(\alpha,\alpha)}\right|=\left|\begin{array}{l}-\dfrac{\alpha\sin\alpha\cos\alpha}{\pi}-\dfrac{(1-\cos\alpha)\sin\alpha}{2}+\dfrac{\pi(\pi\cos\alpha-\pi-2\alpha\cos\alpha+2\sin\alpha)\sin\alpha}{2(8-\pi^2)}\\ -\dfrac{\pi\cos\alpha-\pi-2\alpha\cos\alpha+2\sin\alpha}{8-\pi^2}\end{array}\right| \tag{25}$$

Section D is between section C and B. A peak valve of $Q_{(\varphi,\alpha)}$ occurs at this section. When α is bigger than a certain valve, the distribution state of $Q_{(\varphi,\alpha)}$ likes an inverted letter W. In this case, another peak valve of $Q_{(\varphi,\alpha)}$ occurs at section E which is between section A and C. The derivatives of $Q_{(\varphi,\alpha)}$ with respect to φ at section D and E are both equal to 0.

Then the derivative of $Q_{(\varphi,\alpha)}$ with respect to φ can be calculated by the following expression

$$\frac{\partial Q_{(\varphi,\alpha)}}{\partial\varphi}=\begin{cases}-\cos(\alpha-\varphi)+\dfrac{\alpha\sin\alpha\sin\varphi}{\pi}-\dfrac{(1-\cos\alpha)\cos\varphi}{2}+\dfrac{\pi(\pi\cos\alpha-\pi-2\alpha\cos\alpha+2\sin\alpha)\cos\varphi}{2(8-\pi^2)} & (0\le\varphi<\alpha)\\ \dfrac{\alpha\sin\alpha\sin\varphi}{\pi}-\dfrac{(1-\cos\alpha)\cos\varphi}{2}+\dfrac{\pi(\pi\cos\alpha-\pi-2\alpha\cos\alpha+2\sin\alpha)\cos\varphi}{2(8-\pi^2)} & (\alpha<\varphi\le\pi)\end{cases} \tag{26}$$

When $\dfrac{\partial Q_{(\varphi,\alpha)}}{\partial\varphi}=0$, the position angle φ of section D and E for different α can be calculated, as

shown in Fig .6. The certain valve of α is about 60.3°. Then the value of $\left|Q_{(\varphi,\alpha)}\right|$ at section A, B, C, D and E for different α can be calculated, as shown in Fig .7. The maximal valve of $\left|Q_{(\varphi,\alpha)}\right|$ for different α can be only at section A, B or C. When $0° \le \alpha \le 46.3°$, the maximal valve of $\left|Q_{(\varphi,\alpha)}\right|$ is at section A. When $46.3° < \alpha \le 62.5°$ or $79.5° < \alpha \le 90°$, the maximal valve of $\left|Q_{(\varphi,\alpha)}\right|$ is at section C. When $62.5° < \alpha \le 79.5°$, the maximal valve of $\left|Q_{(\varphi,\alpha)}\right|$ is at section B. The derivative of $\left|Q_{(\varphi,\alpha)}\right|$ with respect to φ at section A, B, C, D and E for different α can be calculated

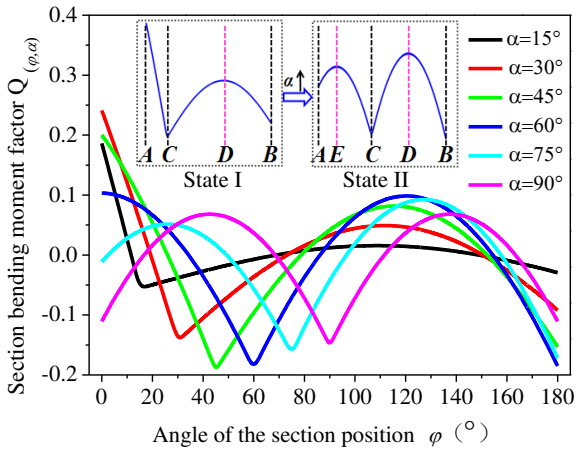

Fig. 5. Relationship between φ, α and $Q_{(\varphi, \alpha)}$.

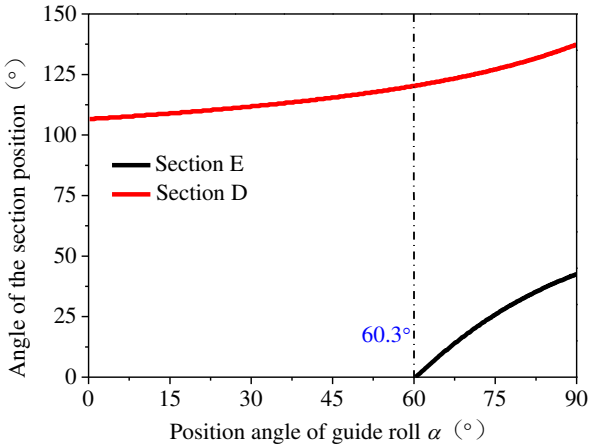

Fig. 6. Position of section E and D under different α

The derivative of $\left|Q_{(\varphi,\alpha)}\right|$ with respect to α at section A, B and C can be calculated, as shown in Fig .8. As it can be seen, the maximal valve of $\left|Q_{(\varphi,\alpha)}\right|$ at section A occurs when α=30°. For section B, the maximal valve occurs when α=63.6°. And for section C, the maximal valve occurs when α=51.5°. Finally, the maximal absolute valve of the section bending moment factor

$\left|Q_{(\alpha,\varphi)}\right|_{max}$ for different α can be calculated, as shown in Fig .9. It can be seen the valve of $\left|Q_{(\alpha,\varphi)}\right|_{max}$ depends on the position angle of guide roll α. The maximal valve of $\left|Q_{(\alpha,\varphi)}\right|_{max}$ occurs when α=30° . When $0° \le \alpha \le 30°$, $46.3° < \alpha \le 51.5°$ or $62.5° < \alpha \le 63.6°$, the valve of $\left|Q_{(\alpha,\varphi)}\right|_{max}$ increases with position angle of guide roll. And when $30° \le \alpha \le 46.3°$, $51.5° < \alpha \le 62.5°$ or $63.6° < \alpha \le 90°$, the valve of $\left|Q_{(\alpha,\varphi)}\right|_{max}$ decreases with position angle of guide roll. Therefore, the influence of $\left|Q_{(\alpha,\varphi)}\right|_{max}$ to the ring stiffness can be come down to the position angle of guide roll α. As we can see, the position angle of guide roll α has a complex influence to the ring stiffness. When the position angle of guide roll α is smaller than 30º, the ring stiffness is weakened as α increasing. And when α is bigger than 30º, the ring stiffness can be improved generally as α increasing. However, the ring stiffness is weakened when $46.3° < \alpha \le 51.5°$ or $62.5° < \alpha \le 63.6°$.

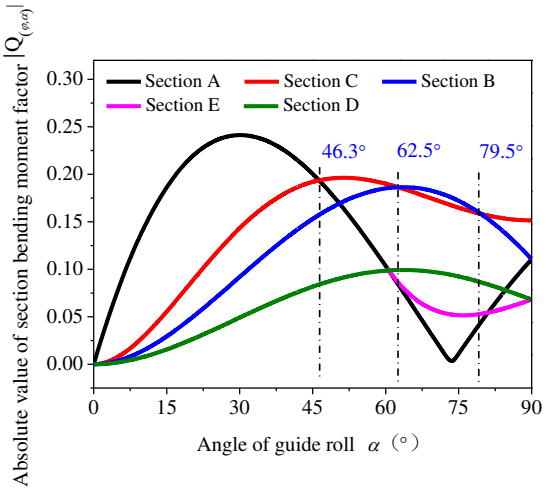

Fig. 7. Relationship between α and $\left|Q_{(\varphi,\alpha)}\right|$ for different sections

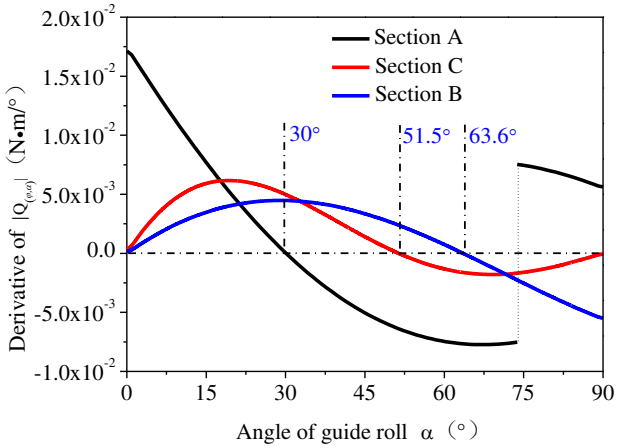

Fig. 8. Derivative of $\left|Q_{(\varphi,\alpha)}\right|$ under different α for section A, B and C

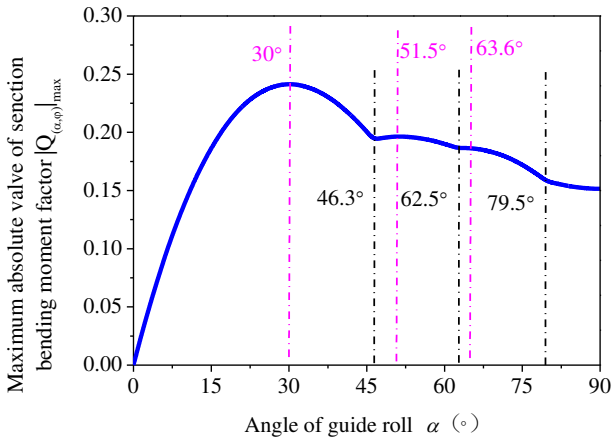

Fig. 9. Values of $\left|Q_{(\varphi,\alpha)}\right|_{max}$ under different α

2.3 Verification by FE simulation

To verify the result above, a static FE simulation for a half circular beam is made in ABAQUS. The all degrees of freedom at the two ends of the half circular beam A and B are limited. The load applied by guide roll to ring is on section C with two component forces F_x and F_y respectively in direction x and y, as shown in Fig. 10(a). The valve of the resultant force of F_x and F_y is equal to the guide force F_g and the direction is pointed to the center of the circle. A rectangular profile is selected for the beam, as shown in Fig. 10(b). The yield strength of the ring material is 40 MPa. The elastic modulus is 116.7449GPa. And the poisson ratio is 0.3. The element type is selected as beam element B31.

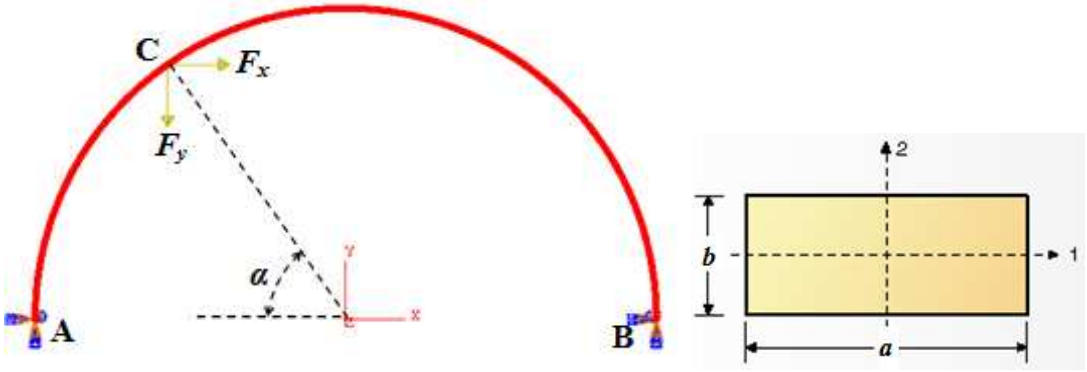

(a) (b)

Fig. 10. A static FE model for a half circular beam: (a) FE model; (b) section shape.

When the average radius of the circular beam R_a=4.596 m, the length of the profile a=0.308 m and the width b=0.308 m, the angle of the guiding force α =22.66 °, the resultant force of F_x and F_y is equal to 2.5×10^5 N, the simulation results are shown in Fig. 11. It can be seen the beam produced plastic bending deformation which meant the stiffness of the beam is destroyed. The maximum stress and strain occur at section A. So a further study about the relationship between the guiding force and the deformation performance at section A is made, as shown in Fig. 12. When the guiding force increases to 1.85×10^5 N, the Mises stress at section A reaches the yield strength and the material begins to produce plastic bending deformation. According to Eq. (22), the maximum allowed guiding force $F_{g\text{-}max}$ can be calculated, the valve is 1.853×10^5 N. Thus it indicates the proposed stiffness model can predict the maximum allowed guiding force accurately.

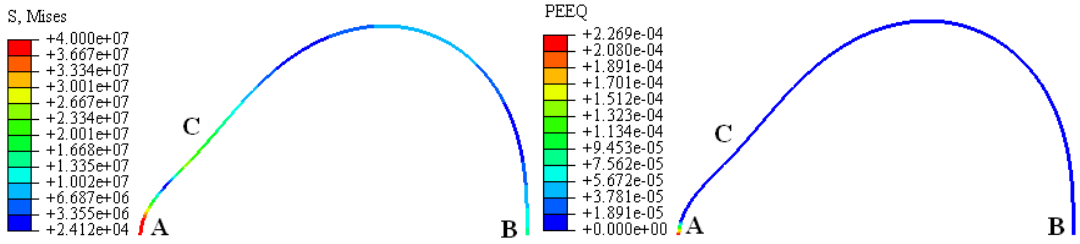

(a) (b)

Fig. 11. Distribution of stress and strain on the beam: (a) equivalent stress; (b) equivalent strain.

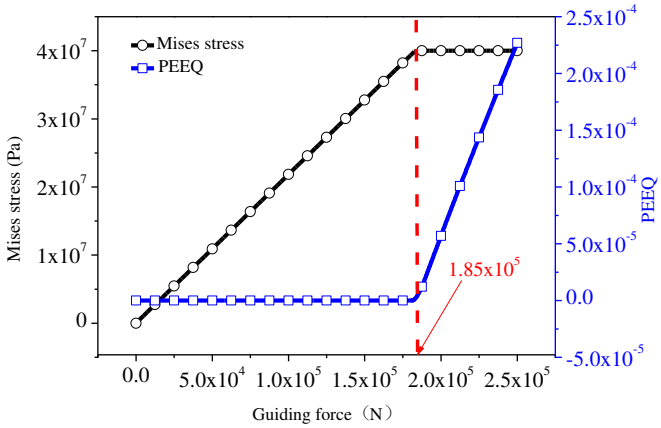

Fig. 12. Evolution of Mises stress and equivalent plastic strain under different guiding force.

Based on the FE model above, when the resultant force of F_x and F_y is equal to 1.85×10^5 N, it is a critical state to produce plastic instability. The simulative results of section bending moment and stress are shown in Fig. 13. According to Eqs. (18) and (20), the theoretical results of section bending moment and stress can be calculated. Fig. 14 shows a comparison of simulative and theoretical results of section bending moment and stress. It can be found the results have a good agreement.

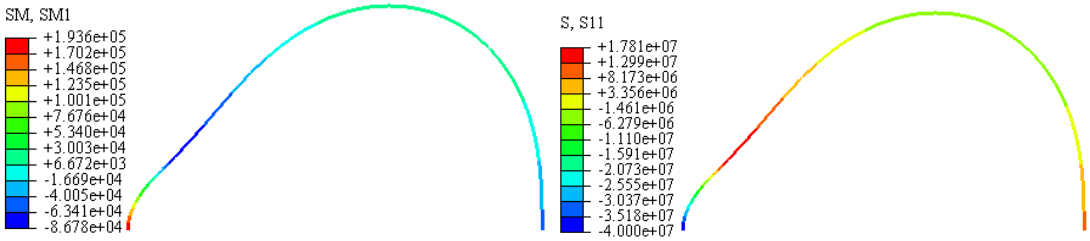

(a) (b)

Fig. 13. Simulative results of section bending moment and stress: (a) section bending moment; (b) section bending stress.

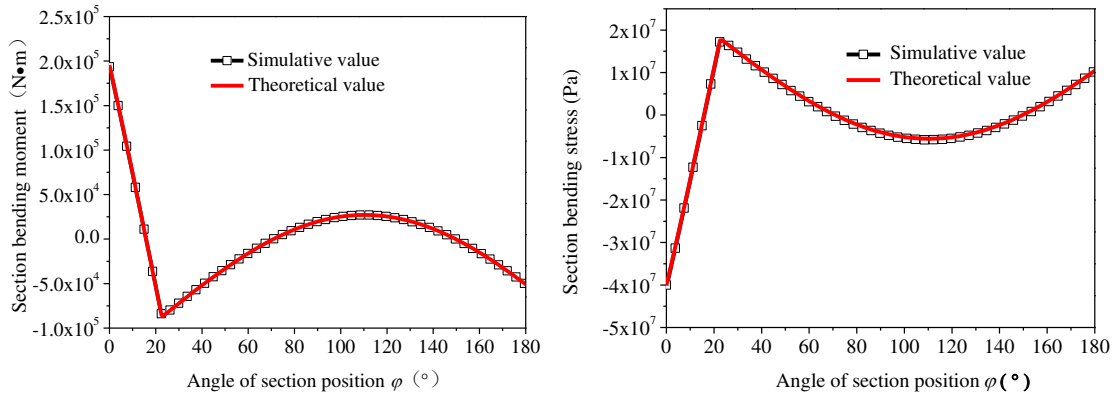

(a) (b)

Fig. 14. Comparison of simulative and theoretical results of section bending moment and stress: (a) section bending moment; (b) section bending stress.

According to Eq. (21), the maximum section bending stress for a ring with certain size and material mainly depends on $\left|Q_{(\varphi,\alpha)}\right|_{\max}$. According to Fig. 7, it can be seen the maximum valve of $\left|Q_{(\varphi,\alpha)}\right|$ occurs at different position when the position angle of guide roll α changes. Thus, to make the beam produce plastic deformation under different angles of guiding force is tried. The simulative result is shown in Fig. 15. As it can be seen when α= {22.66 °, 50 °, 70 °, 90 °}, the earliest position to produce plastic deformation is respectively at section A, section C, section B, section C. And from Fig. 7, the following law can be found. When $0° \le \alpha \le 46.3°$, the maximal valve of $\left|Q_{(\varphi,\alpha)}\right|$ is at section A. When $46.3° < \alpha \le 62.5°$ or $79.5° < \alpha \le 90°$, the maximal valve of $\left|Q_{(\varphi,\alpha)}\right|$ is at section C. When $62.5° < \alpha \le 79.5°$, the maximal valve of $\left|Q_{(\varphi,\alpha)}\right|$ is at section B. Thus, this law can explain the phenomenon appearing in Fig. 15.

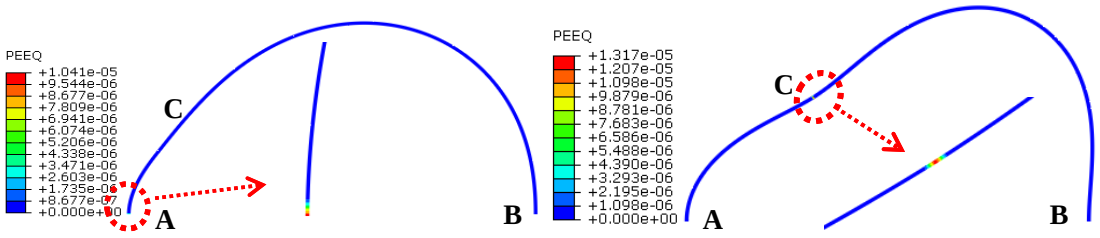

(a) (b)

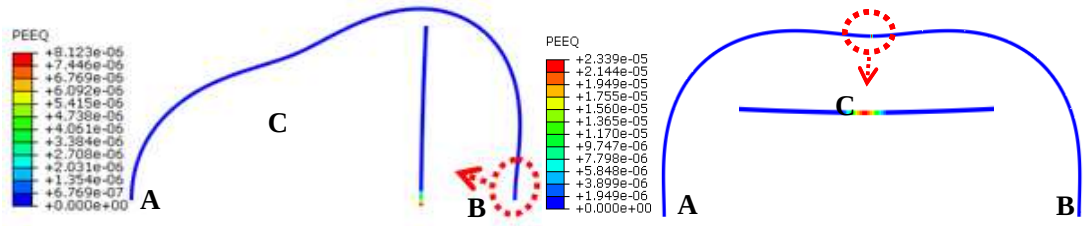

(c) (d)

Fig. 15. The earliest position to produce plastic deformation: (a) α=22.66 °, F_g=1.85×10^5 N; (b) α=50 °, F_g=2.2×10^5 N; (c) α=70 °, F_g=2.4×10^5 N; (d) α=90 °, F_g=2.9×10^5 N.

2.4 Comparison of different ring stiffness models

Recently, scholars have proposed some stiffness models for RARR. In this section, a comparison between some typical models and our model is made.

The stiffness model proposed by Xu et al. (X-model) [31] can be described as the following formula

$$F_g \le F_{Xg-max} = \frac{BH^2\sigma_s}{R_a} K_{X(\alpha)} \tag{27}$$

where $F_{Xg\text{-}max}$ is the maximum allowed guiding force based on X-model, the coefficient

$$K_{X(\alpha)} = \frac{1}{2\sin\alpha}\left\{1+\sin\frac{\alpha}{2}\left[1+\left(\frac{1+\sin\frac{\alpha}{2}}{\cos\frac{\alpha}{2}}\right)^2\right]\right\}.$$

The stiffness model proposed by Hua et al. (H-model) [32] can be described as the following formula

$$F_g \le F_{Hg-max} = \frac{BH^2\sigma_s}{R_a} K_{H(\alpha)} \tag{28}$$

where $F_{Hg\text{-}max}$ is the maximum allowed guiding force based on H-model, the coefficient $K_{H(\alpha)} = \frac{1}{6\sin\alpha}$.

To make an easy comparison, the stiffness model proposed by us (D-model) can be also described as the following formula

$$F_g \le F_{Dg-max} = \frac{BH^2\sigma_s}{R_a} K_{D(\alpha)} \tag{29}$$

where $F_{Dg\text{-}max}$ is the maximum allowed guiding force based on D-model, the coefficient $K_{D(\alpha)} = \frac{1}{6\left|Q_{(\alpha,\varphi)}\right|_{max}}$.

As it can be seen, the forms of the stiffness models above are similar. The difference is in the coefficient $K_{(\alpha)}$, which is a function of α. When α increases from 0 ° to 180 °, the coefficient $K_{(\alpha)}$ for the three models can be calculated, as shown in Fig. 16. It shows that all the valves of coefficient $K_{(\alpha)}$ have a fast decrease when α is smaller than 15 °, and then become a steady level. Besides, the valve of $K_{D(\alpha)}$ is between the valves of $K_{X(\alpha)}$ and $K_{H(\alpha)}$.

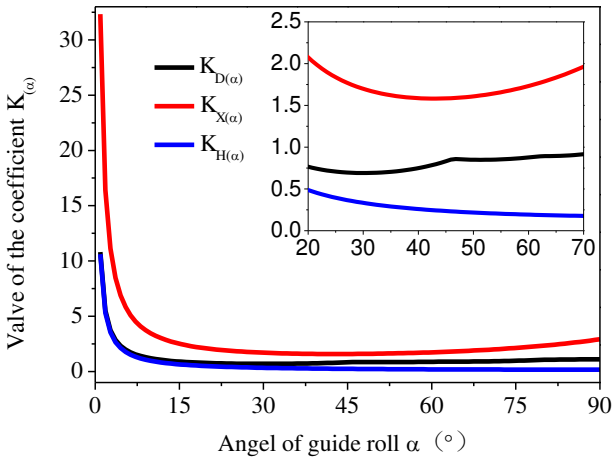

Fig. 16. Comparison of the coefficient $K_{(\alpha)}$ for the three models.

To make a further comparison of the predicted accuracy of the three models above, the maximum allowed guiding force based on the three models can be calculated, according to Eqs. (27), (28) and (29). The angle of guide roll and the geometry size of the ring are two important factors to the maximum allowed guiding force. So the maximum allowed guiding force under different angles of guide roll and geometry sizes of a ring during rolling process for the three models are analyzed. Furthermore, corresponding FE simulations based on Section 2.3 are made. To make an easy comparison of the predicted accuracy of the three models, the ratios of the theoretical values based on the three models to the simulative valves are calculated, as shown in Fig. 17. It

indicates the results of D-model have a good agreement with the simulative results. The results of X-model are bigger than the simulative results and the results of H-model are smaller than the simulative results. In addition, the angel of guide roll has a little influence to the accuracy for D-model, but an obvious influence for X-model and P-model. A larger ring size has a better accuracy for D-model and H-model, but a worse accuracy for X-model.

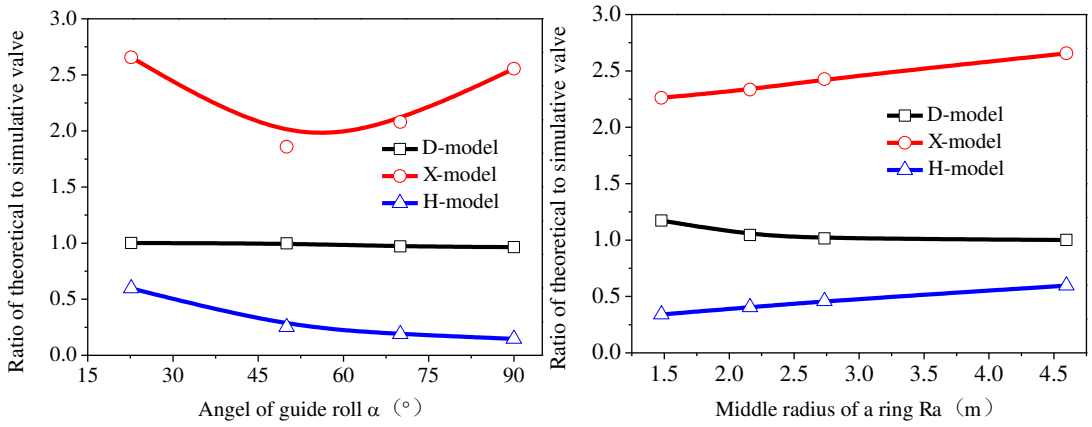

(a) (b)

Fig. 17. Comparison of the predicted accuracy of the maximum allowed guiding force for the three models: (a) under different angles of guide roll; (b) under different radiuses of a ring.

3 Application of ring stiffness model for RARR

3.1 Theoretical analysis

For RARR mill, the movement of guide roll is controlled by the hydraulic cylinder. When the length of the hydraulic cylinder is extended or shortened, the guide roll installed on the swing arm can swing forward or backward around the hinge D, as shown in Fig. 18. The force of guide roll F_g applied on the ring is controlled by adjusting the pressure p in the hydraulic cylinder. Therefore, it is necessary to establish a relationship between p and F_g.

International Journal of Machine Tools & Manufacture, 110 (2016) 66-79
http://dx.doi.org/10.1016/j.ijmachtools.2016.09.003

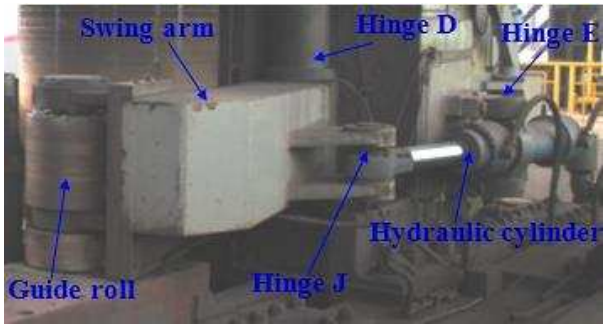

Fig. 18. Mechanical structure of guide roll system in radial-axial ring rolling mill

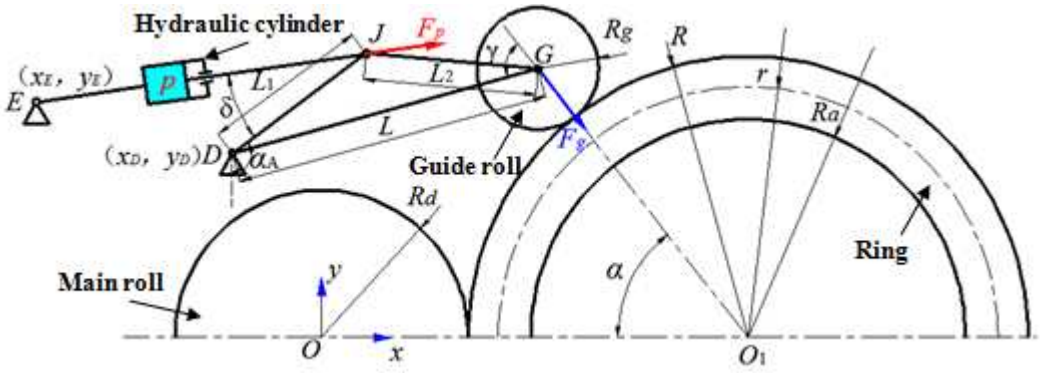

Fig. 19. A simplified structure diagram of guide roll system during ring rolling .

In order to facilitate the analysis, a simplified structure model is adopted, as shown in Fig. 19. To satisfy the mechanical equilibrium condition, the following equation should be ensured

$$F_p L_1 \sin\delta = F_g L \sin\gamma \tag{30}$$

where F_p is the force of hydraulic cylinder, L_1 is the length of beam JD, L is the length of beam DG, γ is the supplementary angel of $\angle DGO_1$, δ is the angel of $\angle DJE$.

According to the geometrical relationship, the valves of γ and δ can be calculated by the following formulas

$$\gamma = \pi - \arccos\frac{L^2 + (R_g + R)^2 - (R + R_m - x_D)^2 - y_D^2}{2L(R_g + R)} \tag{31}$$

$$\delta = \arccos\frac{L_1^2 + (x_D + L_1\sin\alpha_D - x_E)^2 + (y_D - L_1\cos\alpha_D - y_E)^2 - (x_D - x_E)^2 + (y_D - y_E)^2}{2L_1\sqrt{(x_D + L_1\sin\alpha_D - x_E)^2 + (y_D - L_1\cos\alpha_D - y_E)^2}} \tag{32}$$

where R_g is the radius of the guide roll, R is the outer radius of the ring, R_m is the radius of the main roll, x_D and y_D are the coordinate of hinge D in direction x and y respectively, x_E and y_E are the coordinate of hinge E in direction x and y respectively, the angle α_D is given by

$$\alpha_D = \arctan\frac{R+R_m-x_D}{y_D} + \arccos\frac{y_D^2+(R+R_m-x_D)^2+L^2-(R_g+R)^2}{2L\sqrt{y_D^2+(R+R_m-x_D)^2}} + \arccos\frac{L^2+L_1^2-L_2^2}{2LL_1} \quad (33)$$

where L_2 is the length of beam JG.

Finally, the pressure p in the hydraulic cylinder can be expressed as

$$p = \frac{F_g L\sin\gamma}{\pi r_h^2 L_1 \sin\delta} \quad (34)$$

where r_h is the inner radius of the hydraulic cylinder.

Therefore, if the suitable force of guide roll F_g applied on the ring can be determined, the pressure p in the hydraulic cylinder can be also determined. From the analysis above, it can be seen the maximum allowed guiding force $F_{g\text{-}max}$ is determined by Eq. (22). So the pressure p should satisfy the following condition

$$p \le p_{max} = \frac{BH^2\sigma_s L\sin\gamma}{6\pi R_a \left|Q_{(\alpha,\varphi)}\right|_{max} r_h^2 L_1 \sin\delta} \quad (35)$$

Thus, during RARR, the pressure p can be set as

$$p = k_g p_{max} = \frac{k_g BH^2\sigma_s L\sin\gamma}{6\pi R_a \left|Q_{(\alpha,\varphi)}\right|_{max} r_h^2 L_1 \sin\delta} \quad (36)$$

where k_g is an adjustment coefficient and $0 < k_g \le 1$.

Therefore, the force applied on the guide roll can be determined by

$$F_g = k_g F_{g-max} = \frac{k_g BH^2\sigma_s}{6R_a \left|Q_{(\alpha,\varphi)}\right|_{max}} \quad (37)$$

3.2 FE analysis

Based on the theoretical analysis above, in this section, FE simulation for RARR of a super-large ring is carried out. The dimension of the ring and other primary rolling parameters are shown in Table 1. The material of the ring is 42CrMo, and its true stress-strain curves at different temperature T and strain rate $\dot{\varepsilon}$ are shown in Fig. 20. The physical properties including thermal conductivity, specific heat capacity, etc. are provided by Pan [33]. The key technologies for FE

modeling of RARR are referenced to Zhou [25].

Table 1 Primary rolling parameters.

Parameters	values
Diameter of main roll D_m (mm)	1350
Diameter of mandrel D_{m1} (mm)	600
Diameter of guide rolls D_g (mm)	500
Angle of the axial rolls γ (º)	35
Outer diameter of blank D_0 (mm)	3500
Inner diameter of blank d_0 (mm)	2412
Axial height of blank B_0 (mm)	544
Outer diameter of rolled ring D (mm)	9500
Inner diameter of rolled ring d (mm)	8884
Axial height of rolled ring B (mm)	308
Temperature of rolls (℃)	80
Temperature of blank (℃)	1100
Temperature of environment (℃)	20
Heat transmission coefficient ($N\cdot s^{-1}\cdot mm\text{-}1\cdot ℃^{-1}$)	10
Heat convection coefficient ($N\cdot s^{-1}\cdot mm\text{-}1\cdot ℃^{-1}$)	0.02
Heat radiation coefficient ($N\cdot s^{-1}\cdot mm^{-1}\cdot ℃^{-4}$)	0.7
Friction coefficient	0.3

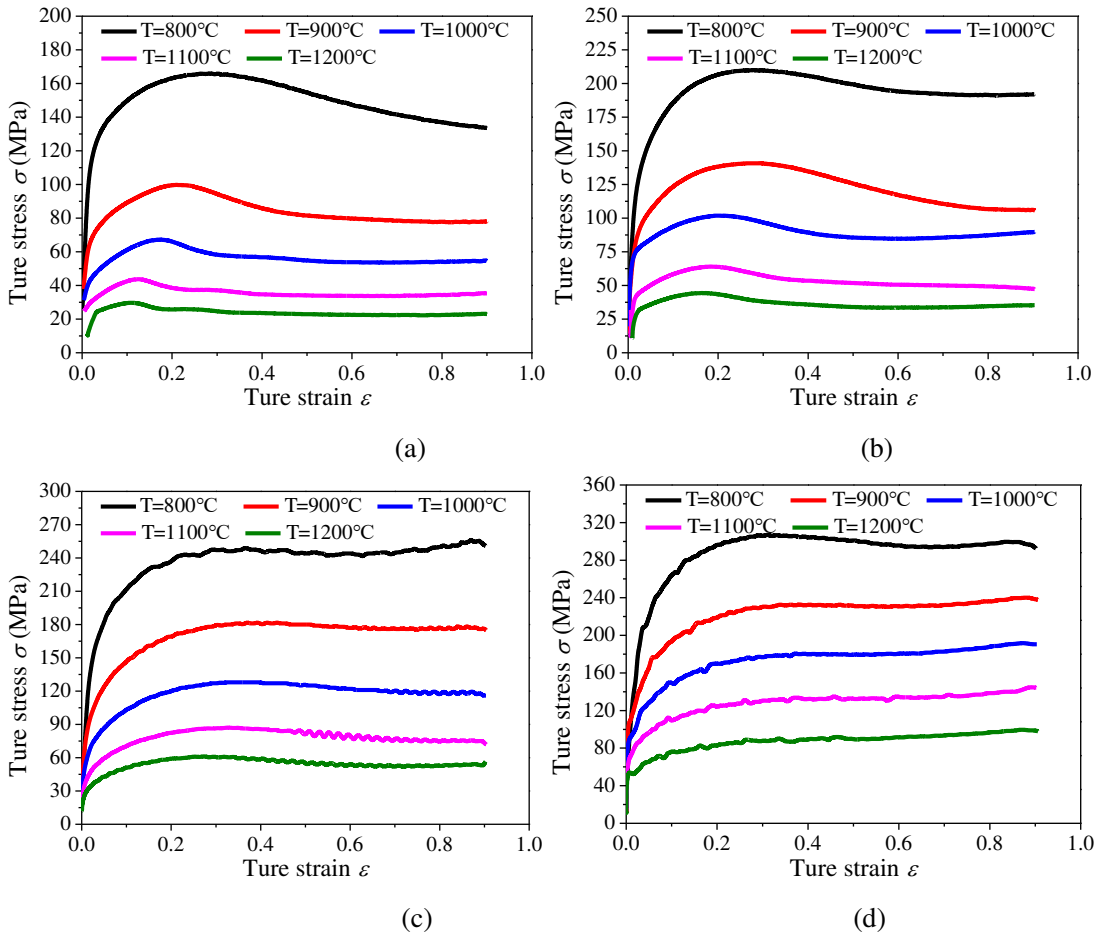

Fig. 20. True stress-strain curves of 42CrMo at different temperature T and strain rate $\dot{\varepsilon}$: (a)

$\dot{\varepsilon}$=0.01; (b) $\dot{\varepsilon}$=0.1; (c) $\dot{\varepsilon}$=1; (d) $\dot{\varepsilon}$=10 [22].

From Fig. 20, it can be seen the stress is varied with strain, strain rate and temperature. During RARR, the temperature in the ring surface area decreases, but in the ring center area it keeps almost constant. Thus, the strength of the material increases gradually in a certain extent during rolling process. However, to simplify the calculation, the stress at initial temperature (1100 ℃) is selected as a basis. In addition, the unstable deformation generally happens at a low strain rate. So the stress level of the material is selected at T= 1100 ℃ and $\dot{\varepsilon}$=0.01, the strength valve is about 40 MPa. Combined with the dimension of the ring and rolling mill, the theoretical pressure in hydraulic cylinder and force applied on the guide roll can be calculated according to Eqs. (36) and (37). The result when k_g=1 is shown in Fig. 21. It can be found the pressure in hydraulic cylinder and force applied on the guide roll should be reduced gradually during rolling process.

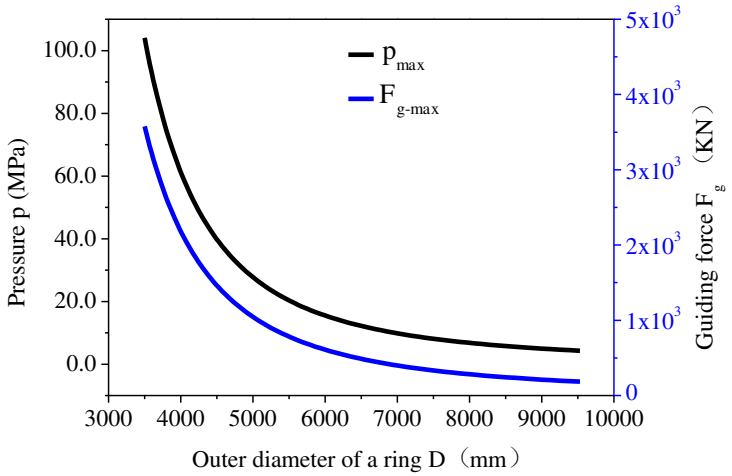

Fig. 21. Theoretical pressure in hydraulic cylinder and force applied on the guide roll during RARR.

To simplify the FE model, the guide roll is connected with a swing arm. The swing arm can revolve around an endpoint. A equivalent moment is applied on the endpoint to simulate the force applied on the guide roll, as shown in Fig. 22. The equivalent moment can be calculated by the following expression

$$M_A = F_g L \sin\gamma = \frac{k_g B H^2 \sigma_s L \sin\gamma}{6 R_a \left| Q_{(\alpha,\varphi)} \right|_{max}} \tag{38}$$

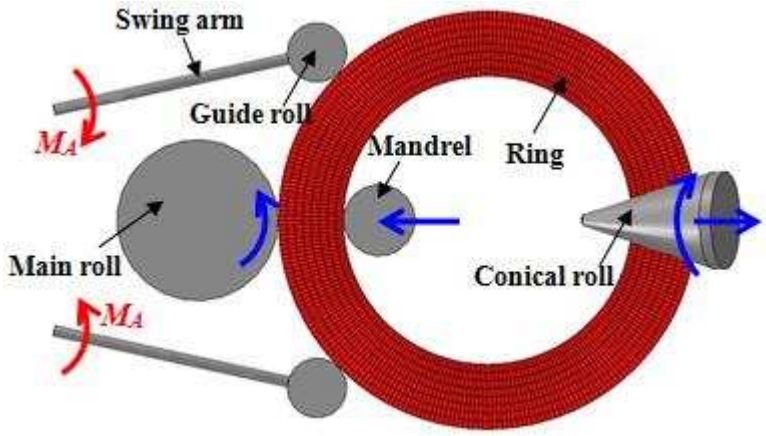

Fig. 22. 3D FE model for RARR.

When k_g=1, the valve of the equivalent moment during rolling process is shown in Fig. 23. It shows the moment is relatively large at initial rolling stage, and then it reduces gradually as the ring diameter enlarging.

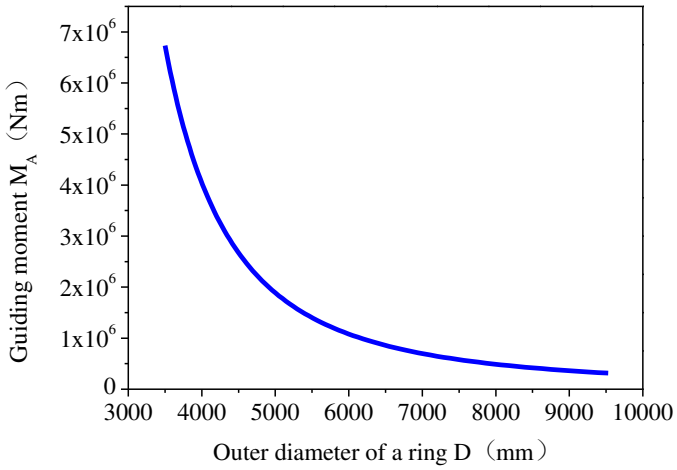

Fig. 23. Theoretical guiding moment applied on the guide roll during RARR.

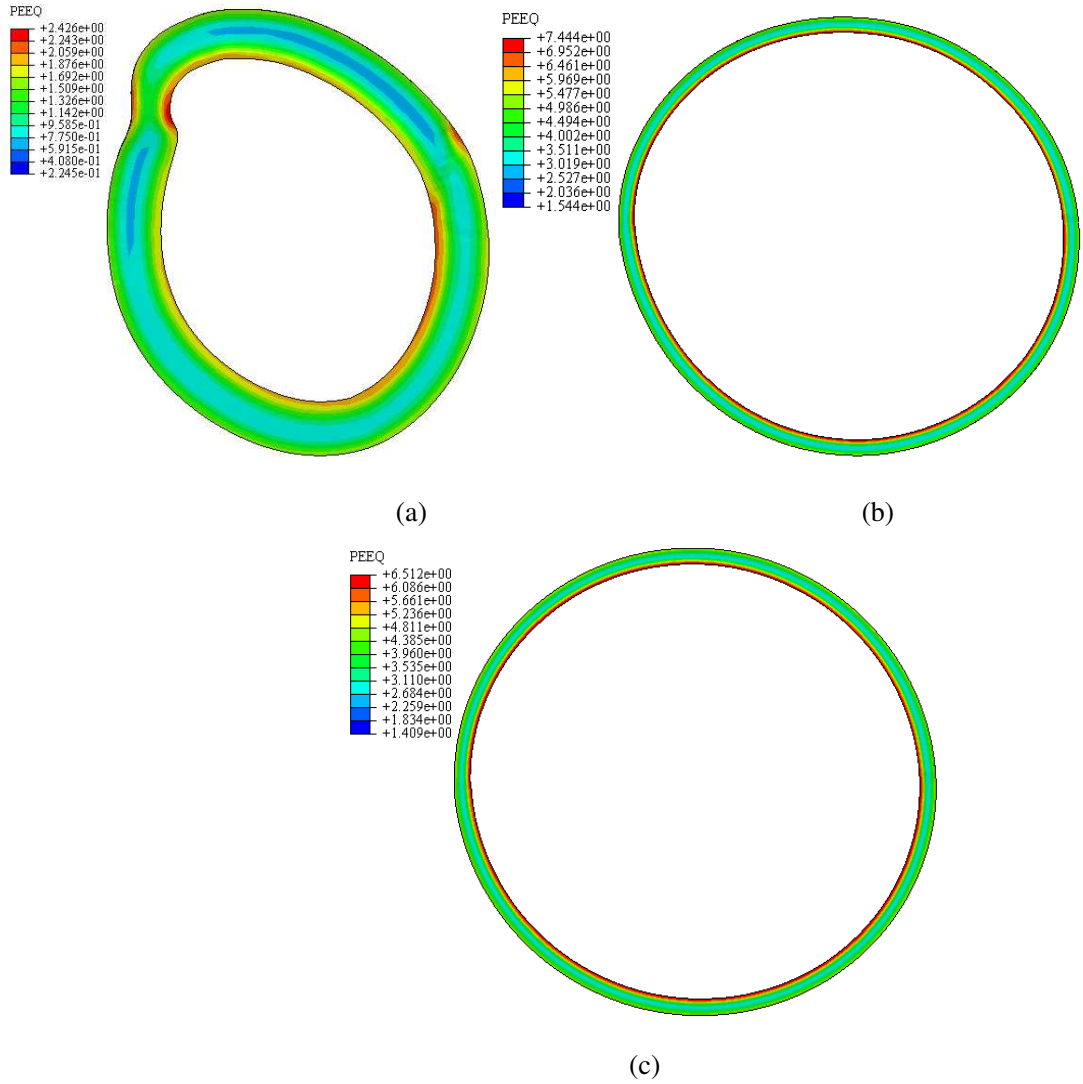

Fig. 24. Forming results of the ring after RARR: (a) k_g=1.5; (b) k_g=1; (c) k_g=0.2.

Fig. 24. shows the forming results of the ring after RARR when selecting different valves of k_g. It can be seen the ring is destroyed when k_g =1.5. As the force applied on the guide roll is too large, more than the maximum allowed force. The stiffness condition cannot be satisfied. So the ring produces bending deformation, and the failure shape is similar to Fig. 2. This phenomenon reflects the accuracy of the theoretical stiffness model in a certain extent. When k_g =1, the ring produces little bending deformation, but it is not obvious and the rolling process can finish. When k_g =0.2, the shape of the ring is good and the rolling process is stable. Therefore, the force applied on the guide roll should slightly smaller than the maximum allowed valve.

To make a further study on the suitable guiding force, a range of the adjustment coefficient k_g

from 0.02 to 1 is selected. When the guiding force is changed, the shape of the ring may be changed during rolling process. Thus, the roundness error e_R is introduced to evaluate the ring roundness. It can be defined as

$$e_R=\sqrt{\frac{\sum_{i=1}^{n}(R_i-R_a)^2}{n}} \tag{39}$$

where n is the number of selected points on the ring outer surface, R_a is the average outer radius of the ring, R_i is the outer radius at point i.

Fig. 24. describes the roundness of the ring during RARR under different adjustment coefficients. It can be seen when the adjustment coefficients k_g is selected too large or small, the roundness error of the ring increases. Larger guiding force can make the ring produce bending deformation, leading to the ring unstable. Smaller guiding force cannot support the ring in a stable status, leading to the ring wagging. Therefore, the adjustment coefficients k_g should be selected in an appropriate range to offer a suitable guiding force. It can be found when the adjustment coefficient k_g is selected in a range of 0.1 to 0.5, the ring roundness error can be kept in a lower level. That is to say, it is beneficial to form a good shape ring when the pressure p in the hydraulic cylinder is controlled in a suitable level with k_g=0.1~0.5.

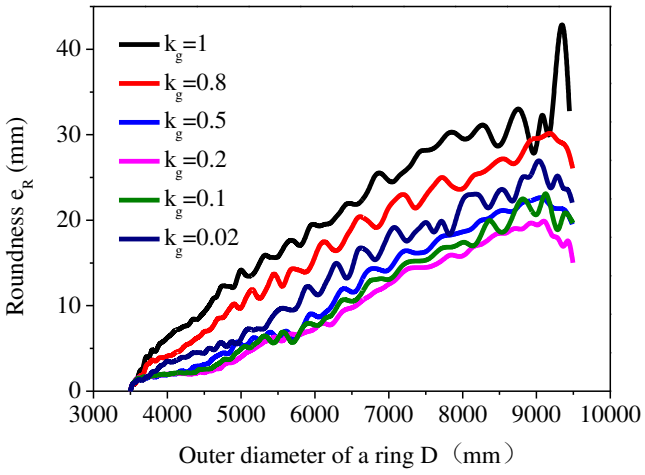

Fig. 25. Roundness of the ring during RARR under different adjustment coefficients.

International Journal of Machine Tools & Manufacture, 110 (2016) 66-79
http://dx.doi.org/10.1016/j.ijmachtools.2016.09.003

3.3 Experimental verification

Through the analysis above, a suitable range of the pressure p in the hydraulic cylinder is determined. Then a rolling experiment for the super-large ring was conducted on a lager RARR mill. The details about the ring and the rolling mill are as the description in Section 3.2. Before ring rolling, the pressure p in the hydraulic cylinder was set in a level when k_g=0.2. The experimental valve waved but kept in a similar level as the set during rolling process, as shown in Fig. 26. By this control method, the rolling process was stable and formed a super-large ring with good dimensional accuracy successfully, as shown in Fig. 27. Thus, it indicates the control method of the pressure p in the hydraulic cylinder based on our stiffness model is feasible.

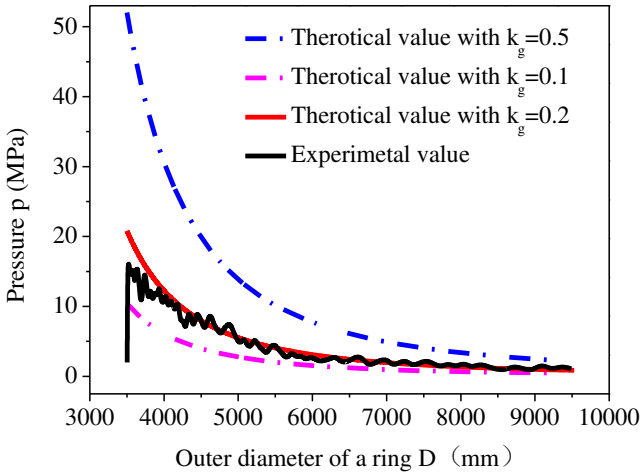

Fig. 26. Theoretical and experimental values of the pressure in hydraulic cylinder.

Fig. 27. Experimental result of RARR for a super-large ring.

4 Conclusions

In this study, a mathematical model of ring stiffness condition for RARR was established

based on the force method. Then the influence factors to ring stiffness were discussed. Furthermore, the predicted results were compared with FE simulation and other ring stiffness models. Based on the stiffness model, a control method of the pressure in the hydraulic cylinder to control the guiding force was proposed and applied in a RARR experiment of a super-large ring successfully. The main conclusions are drawn as follows:

(1) Bigger geometric dimension of ring cross section, smaller geometric dimension of ring radius and bigger yield strength of ring material are good for improving the ring stiffness. When the position angle of guide roll α is smaller than 30º, the ring stiffness is weakened as α increasing. And when α is bigger than 30º, the ring stiffness can be improved generally as α increasing. However, the ring stiffness is weakened when $46.3° < \alpha \le 51.5°$ or $62.5° < \alpha \le 63.6°$.

(2) Compared with FE simulative result, the theoretical result based on our stiffness model has a good agreement. And the predicted result is more accurate than other two stiffness models.

(3) The pressure in hydraulic cylinder and force applied on the guide roll should be reduced gradually during ring rolling process. Through selecting suitable adjustment coefficient k_g to control the pressure in hydraulic cylinder and force applied on the guide roll can keep ring rolling process stable and form a ring with good dimensional accuracy.

Acknowledgments

The authors would like to thank the National Natural Science Foundation of China (No.51135007), the Innovative Research Development Program of Ministry of Education of China (No. IRT13087), the Science and Technology Support Program of Hubei province (No.2014BAA008) and the EU FP7 IRSES project of Marie Curie Actions (PIRSES-GA-2012–318968).

References

[1] J.M. Allwood, A. Erman Tekkaya, T.F. Stanistreet, The development of ring rolling technology, Steel Research, 76 (2) (2005) 111-120.

[2] J.M. Allwood, A. Erman Tekkaya, T.F. Stanistreet, The development of ring rolling technology - part 2: investigation of process behaviour and production equipment, Steel Research 76 (7) (2005) 491-507.

[3] J.B. Hawkyard, W. Johnson, J. Kirhland, E. Appleton, Analyses for roll force and torque in ring rolling with some supporting experiments, International Journal of Mechanical Sciences 15 (11) (1973) 873-893.

[4] L. Hua, Z.Z. Zhao, The extremun parameters in ring rolling, Journal of Materials Processing Technology 69 (1-3) (1997) 273-276.

[5] D.S. Qian, L. Hua, L.B Pan, Research on gripping conditions in profile ring rolling of raceway groove, Journal of Materials Processing Technology 209 (6) (2009) 2794-2802.

[6] K.H. Lee, B.M. Kim, Advanced feasible forming condition for reducing ring spreads in radial–axial ring rolling, International Journal of Mechanical Sciences 76 (2013) 21-32.

[7] N. Kim, S. Machida, S. Kobayshi, Ring rolling process simulation by the three dimension finite element method, International Journal of Machine Tools & Manufacture 30 (4) (1990) 569-577.

[8] H. Yang, M. Wang, L.G. Guo, Z.C. Sun, 3D coupled thermo-mechanical FE modeling of blank size effects on the uniformity of strain and temperature distributions during hot rolling of titanium alloy large rings, Computational Materials Science, 44 (2008) 611-621.

[9] F.L. Yan, L. Hua, Y.Q. Wu, Planning feed speed in cold ring rolling, International Journal of Machine Tools and Manufacture 47(11) (2007) 1695-1701.

[10] Y.M. Zhao, D.S. Qian. Effect of rolling ratio on groove-section profile ring rolling, Journal of

Mechanical Science and Technology, 24 (8) (2010) 1679-1687.

[11] X.K. Wang, L. Hua, Modeling of on-line measurement for rolling the rings with blank size errors in vertical hot ring rolling process, International Journal of Advanced Manufacturing Technology 68 (1-4) (2013) 257-262.

[12] T.F. Stanistreet, J.M. Allwood, A.M. Willoughby, The design of a flexible model ring rolling machine. Journal of Materials Processing Technology 177 (2006) 630-633.

[13] C.L. Xie, X.H. Dong, S.J. Li, S.H. Huang, Rigid–viscoplastic dynamic explicit FEA of the ring rolling process, International Journal of Machine Tools & Manufacture 40 (2000) 81–93.

[14] K. Davey, M.J. Ward, An ALE approach for finite element ring-rolling simulation of profiled rings, Journal of Materials Processing Technology 139 (2003) 559-566.

[15] B. Kim, H. Moon, E.Kim, M. Choi, M. Joun, A dual-mesh approach to ring-rolling simulations with emphasis on remeshing, Journal of Manufacturing Processes 15 (2013) 635-643.

[16] J.T. Yeom, J.H. Kim, J.K. Hong, N. K. Park, C.S. Lee, FE analysis of microstructure evolution during ring rolling process of a large-scale Ti-6Al-4V alloy ring, Materials Science Forum 638-642 (2010) 223-228.

[17] G. Schwich, T. Henke, J. Seitz, G. Hirt, Prediction of microstructure and resulting rolling forces by application of a material model in a hot ring rolling process, Key Engineering Materials 622-623 (2014) 970-977.

[18] S. Zhu, H. Yang, L.G. Guo, W.J. Di, Effects of initial forming temperature on primary alpha evolution during radial-axial ring rolling for TA15 titanium alloy, Procedia Engineering 81 (2014) 274 -279.

[19] G. Zhou, L. Hua, D.S. Qian, D.F. Shi, H.X. Li, Effects of axial rolls motions on radial-axial rolling process for large-scale alloy steel ring with 3D coupled thermo-mechanical FEA,

International Journal of Mechanical Science 59 (1) (2012) 1-7.

[20] G. Zhou, L. Hua, J. Lan, D.S. Qian, FE analysis of coupled thermo-mechanical behaviors in radial-axial rolling of alloy steel large ring, Computational Materials Science 50 (1) (2010) 65-76.

[21] G. Zhou, L. Hua, J. Lan, D.S. Qian, 3D coupled thermo-mechanical FE modeling and simulation of radial-axial ring rolling, Materials Research Innovations, 15 (2011) 221-224.

[22] D.S. Qian, G. Zhou, L. Hua, D.F. Shi, H.X. Li, 3D coupled thermo-mechanical FE analysis of blank size effects on radial-axial ring rolling, Ironmaking & Steelmaking 40 (5) (2013) 360-368.

[23] S. Zhu, H. Yang, L. Guo, L. Hu, X. Chen, Research on the effects of coordinate deformation on radial-axial ring rolling process by FE simulation based on in-process control, The International Journal of Advanced Manufacturing Technology, 72 (2014) 57-68.

[24] D.S. Qian, Y. Pan, 3D coupled macro-microscopic finite element modelling and simulation for combined blank-forging and rolling process of alloy steel large ring, Computational Materials Science 70 (2013) 24-36.

[25] G. Zhou, L. Hua, D.S. Qian, 3D coupled thermo-mechanical FE analysis of roll size effects on the radial-axial ring rolling process, Computational Materials Science 50 (3) (2011) 911-924.

[26] L.G. Guo, H. Yang, Towards a steady forming condition for radial-axial ring rolling, International Journal of Mechanical Sciences 53 (4) (2011) 286-299.

[27] F.L. Yan, L. Hua, Y.Q. Wu, Planning feed speed in cold ring rolling, International Journal of Machine Tools and Manufacture 47 (11) (2007) 1695-1701.

[28] L.Y. Li, H. Yang, L.G. Guo, Z.C. Sun. A control method of guide rolls in 3D-FE simulation of ring rolling, Journal of Materials Processing Technology 205 (1-3) (2008) 99-110.

[29] Z.H. Xu, D. Zhao, Q. Wang, Plastic instability criterion of radial ring rolling, Advanced Materials Research 690-693 (2013) 2352-2355.

[30] M.R. Forouzan, M. Salimi, M.S. Gadala, A.A. Aljawi. Guide roll simulation in FE analysis of ring rolling. Journal of Materials Processing Technology 142 (2003) 213–223.

[31] S.G. Xu, J.C. Lian, A method to find the most suitable angle of guide roll in ring rolling, Metalforming Machinery (6) (1991) 22-25 (in Chinese)

[32] L. Hua, L.B. Pan, J. Lan, Researches on the ring stiffness condition in radial–axial ring rolling, Journal of Materials Processing Technology 209 (5) (2009) 2570-2575.

[33] J.Z. Pan, Pressure vessel material practical manual, Chemical Industry Press, Beijing, China, 2000. (in Chinese)